Supporting Information

Mitigation of RuO_6 Octahedron Distortion by Enhanced A-site Electronegativity in Pyrochlore for Acidic Water Oxidation

Jiabiao Yan[a, +], Jing Zhu[c, +], Dawei Chen[a, *], Shuai Liu[d], Xu Zhang[a], Shoushan Yu[a, *], Zhenhua Zeng[b, *], Luhua Jiang[a, *], Fanglin Du[a]

a. College of Material Science and Engineering, Qingdao University of Science and Technology, Zhengzhou Road 53, Qingdao, 266042, China. E-mail: D. Chen (daweichen@qust.edu.cn), L. Jiang (luhuajiang@qust.edu.cn), S. Yu (shoushanyu@qust.edu.cn)

b. Davidson School of Chemical Engineering, Purdue University, West Lafayette, IN 47907, USA. E-mail: Z. Zeng (zeng46@purdue.edu)

c. Department of Chemical Physics, School of Chemistry and Materials Science, University of Science and Technology of China, Hefei 230026, Anhui, China.

d. School of Mechatronics and Energy Engineering, Ningbo Institute of Technology, Zhejiang University, Ningbo, 315100, China.

Electrochemical Measurements.

In order to calculate the geometric current density (j_{geo}), the current was normalized by the geometric area of GCE according to the Equation 1:

$$j_{geo} = \frac{i \times 1000}{S} \quad (mA/cm^2) \quad (1)$$

where i (A) is the current compensated by 95% iR-drop, and S is the geometric area of GCE (0.19625 cm^2).

In order to calculate the ruthenium mass activity (j_{Ru}), the current was normalized by the mass of ruthenium according to the Equation 2:

$$j_{Ru} = \frac{i \times 1000}{S \times m_{loading} \times W_{Ru}} \quad (A/g_{Ru}) \quad (2)$$

where i (A) is the current compensated by 95% iR-drop, S is the geometric area of GCE (0.19625 cm^2), W_{Ru} is weight percent of Ru(wt.%) in the catalyst, and $m_{loading}$ is the loading of catalyst on GCE (0.2 mg cm^{-2}).

ECSA was caculated by the cyclic voltammetry curves with different scanning rates (10, 20, 30, 40, and 50 mV s^{-1}, respectively). The non-Faradaic current measured was plotted as a function of scan rate to obtain the capacitances (Cdl). Then, the ECSA was caculated according to the Equation 3:

$$ECSA = \frac{C_{dl} \times S}{C_S} \quad (cm^2) \quad (3)$$

where C_{dl} is the capacitance for each samples, S is the geometric area of GCE (0.19625 cm^2), the value of specific capacitance (Cs) is 0.035 mF/cm^2 in this work and Cdl/Cs is the roughness factor (RF).

Finally, the OER polarization curves was normalized by ECSA according to the Equation 4:

$$j_{ECSA} = \frac{i \times 1000}{ECSA} \quad (mA/cm^2) \quad (4)$$

where i (A) is the current compensated by 95% iR-drop, and ECSA is the electrochemical active surface area (cm^2) calculated according to the Equation (3).

Polarization curves normalized by BET area (j_{BET}) was obtained according to the Equation (5):

$$j_{BET} = \frac{i \times 1000}{S \times BETarea \times m_{loading}} \quad (mA/cm^2) \quad (5)$$

where i (A) is the current compensated by 95% iR-drop, S is the geometric area of GCE (0.19625 cm^2), BETarea is calculated by the Nitrogen absorption-desorption isotherms, and $m_{loading}$ is the loading of catalyst on GCE (0.2 mg cm^{-2}).

In order to calculate the turnover frequencies (TOFs), we make the following settings. Firstly, assuming each ruthenium atoms in the catalysts formed one active center. The numbers of Ru atoms number in catalysts were calculated from the weight percent of Ru and the mass loading on the glass carbon electrode according to the equation (6):

$$N_{Ru=} \frac{m_{loading} \times S \times W_{Ru}}{M_{Ru} \times 1000} \times N_A \quad (6)$$

where $m_{loading}$ is loading of catalyst (0.2 mg cm^{-2}), S is the geometric area of GCE (0.19625 cm^2), W_{Ru} is weight percent of Ru (wt.%) in the catalyst, M_{Ru} is the molar mass of Ru, and N_A is the Avogadro constant (6.02×10^{23} mol^{-1}).

The number of total O_2 turnovers per second (N_{O_2}/s) was calculated from the current density (j_{geo}) according to the Equation (7):

$$N_{O_2}/s = \frac{j_{geo} \times S}{4e \times 1000} \quad (s^{-1}) \quad (7)$$

where j_{geo} (mA/cm^2) is the current density mormalized by geometric area, S is the geometric area of GCE (0.19625 cm^2), the number of 4 means 4 electrons transfer in OER, and e is the charge of electron (1.6×10^{-19} C).

Thus, the TOF value underestimated was calculated according to the equation (8), assuming the Faraday efficiency of the reation process is 100%.

$$TOF\ (O_2) = \frac{N_{O_2}/s}{N_{Ru}} = \frac{j_{geo} \times M_{Ru}}{m_{loading} \times W_{Ru} \times 4F} \quad (s^{-1}) \quad (8)$$

where j_{geo} (mA/cm^2) is the current density mormalized by geometric area, M_{Ru} is the molar mass of Ru, $m_{loading}$ is the loading of catalyst on GCE (0.2 mg cm^{-2}), W_{Ru} is weight percent of Ru (wt.%) in the catalyst, the number of 4 means 4 electrons transfer in OER, and F is Faraday constant (96485 C mol^{-1}).

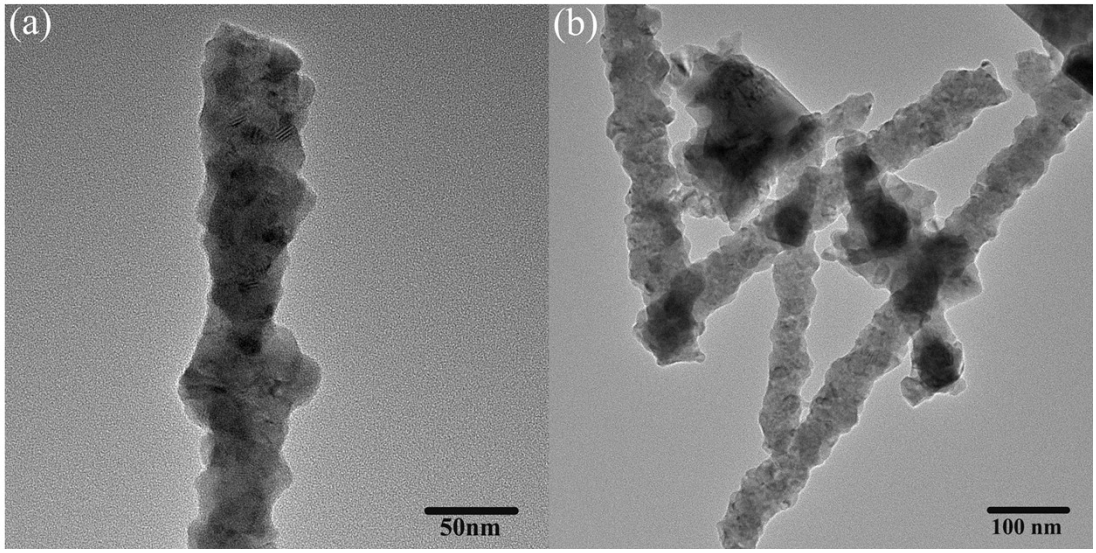

Fig. S1. Transmission electron microscopy (TEM) images of YRO.

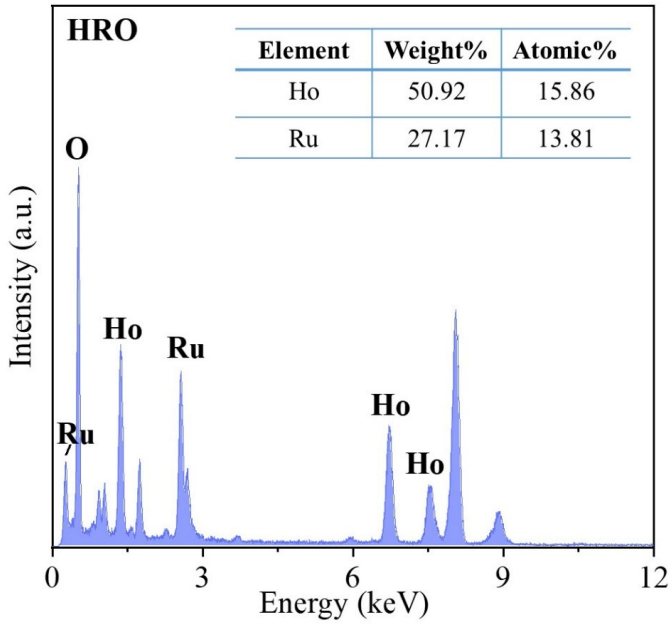

Fig. S2. Transmission electron microscopy with energy dispersive X-Ray spectroscopy (TEM-EDX**)** image of HRO.

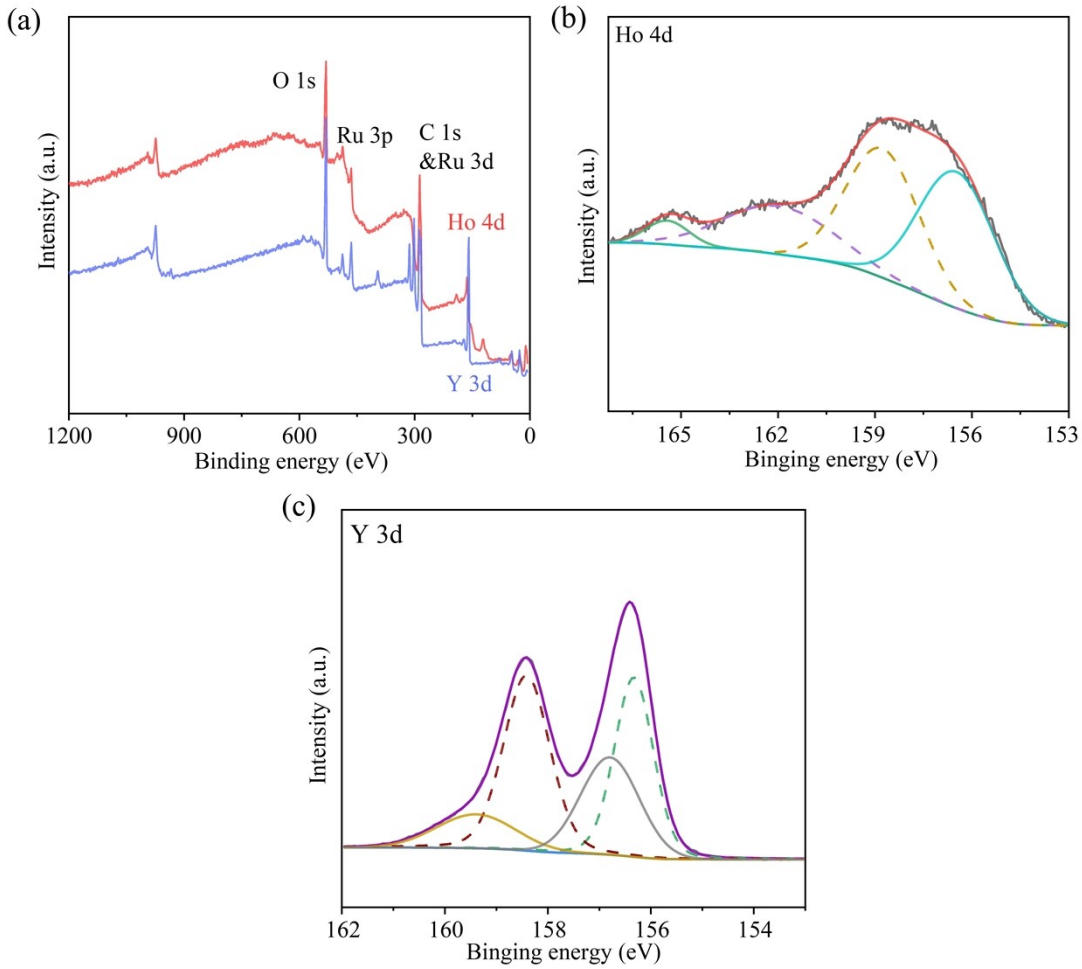

Fig. S3. (a) the wide XPS spectra for HRO and YRO; (b) the XPS spectra of Ho 4d for HRO; (c) the XPS spectra of Y 3d for YRO.

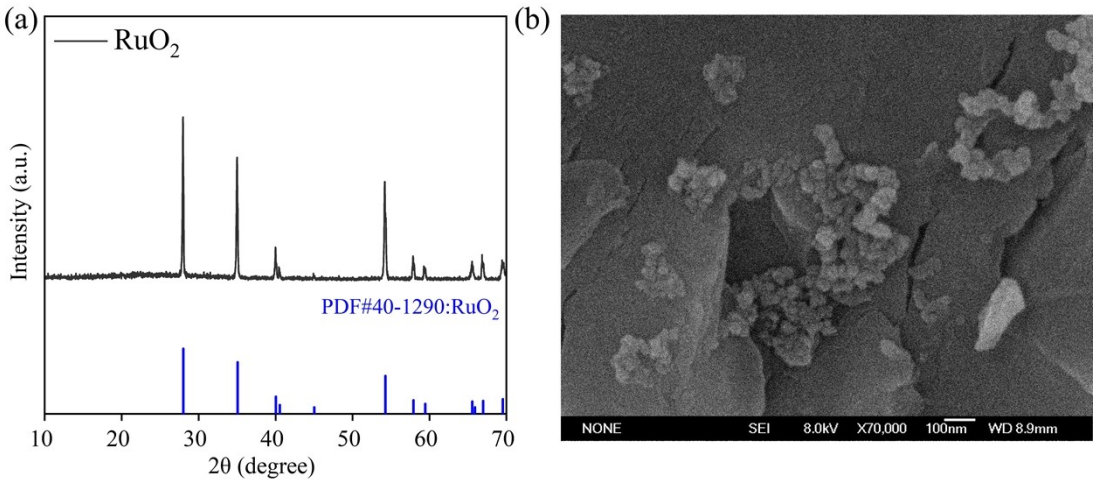

Fig. S4. (a) X-ray diffraction (XRD) and (b) Scanning electron microscope (SEM) images of RuO_2.

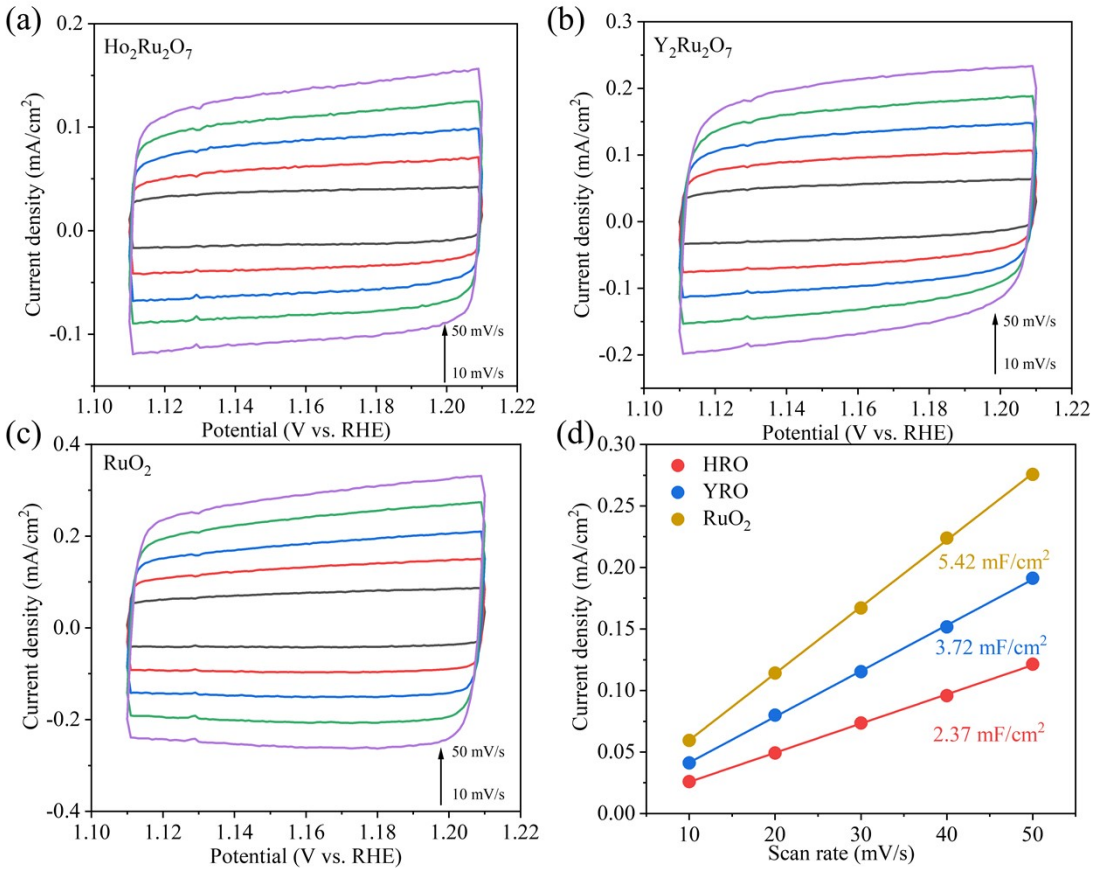

Fig. S5. (a-c) CV scanning curves in 0.1 M $HClO_4$ electrolyte at different scan rates in non-Faradaic potential region for HRO, YRO and RuO_2, respectively; (d) Double-layer capacitances of various catalysts.

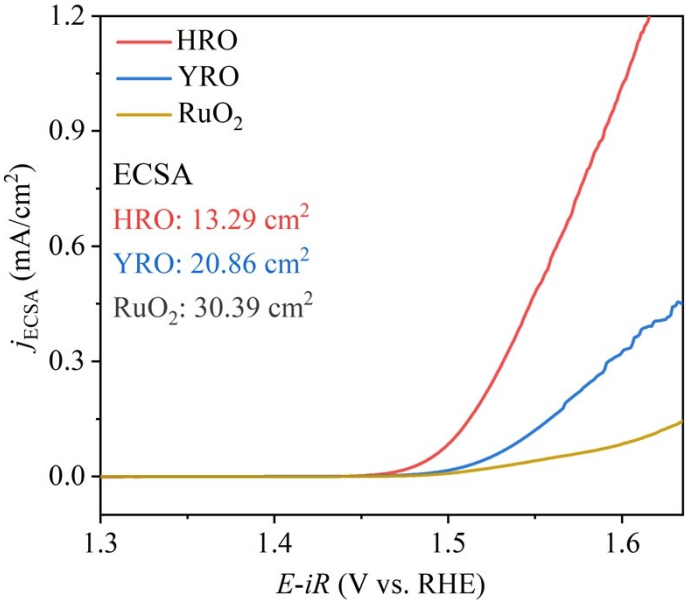

Fig. S6. LSV polarization curves normalized by ECSA.

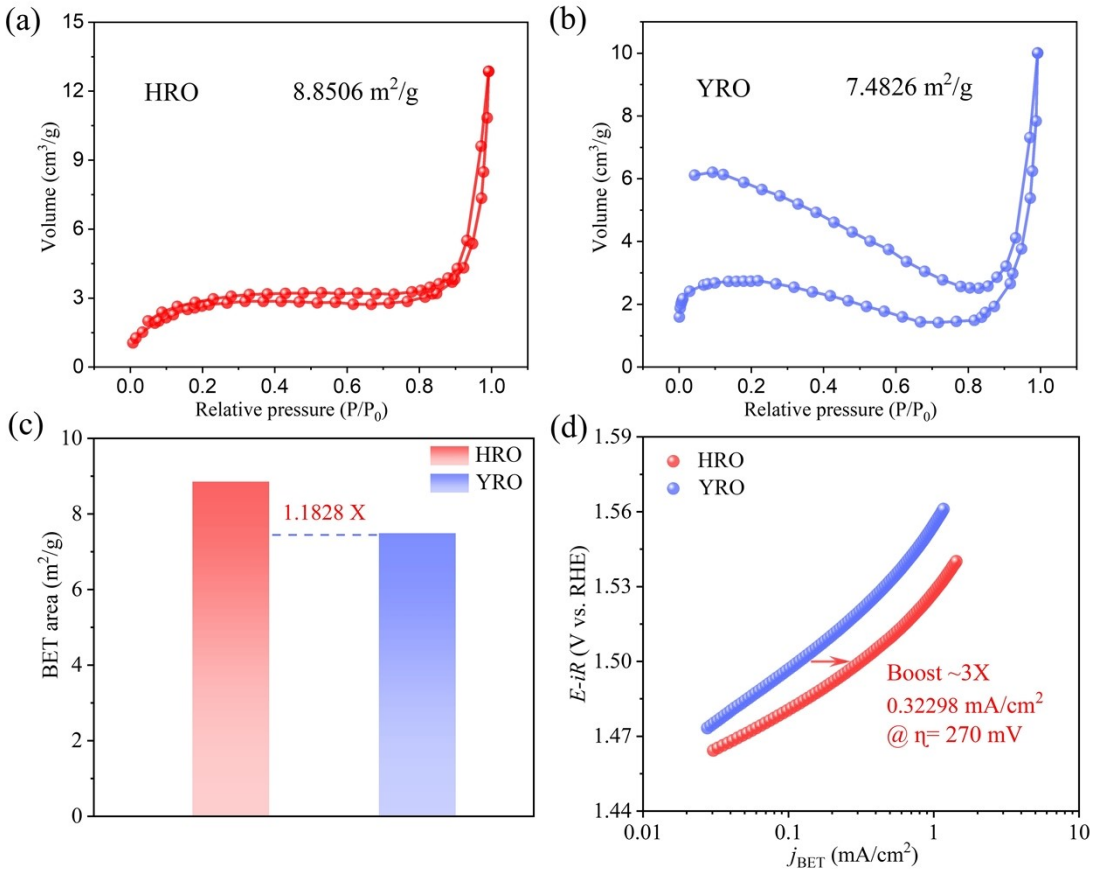

Fig. S7. Nitrogen absorption-desorption isotherms with the corresponding Brunauer-Emmett-Teller (BET) surface area for (a) HRO and (b) YRO; (c) the comparison of BET area for HRO and YRO; (d) polarization curves normalized by BET area.

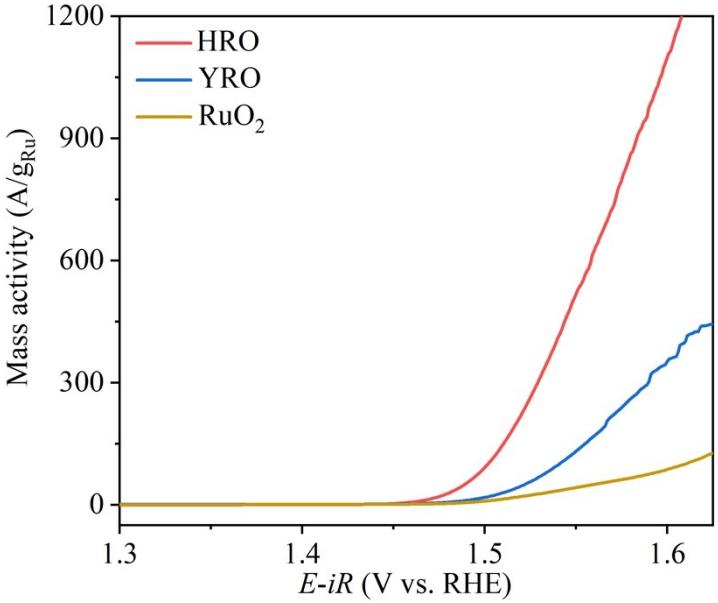

Fig. S8. LSV polarization curves normalized by the mass of ruthenium in catalyst.

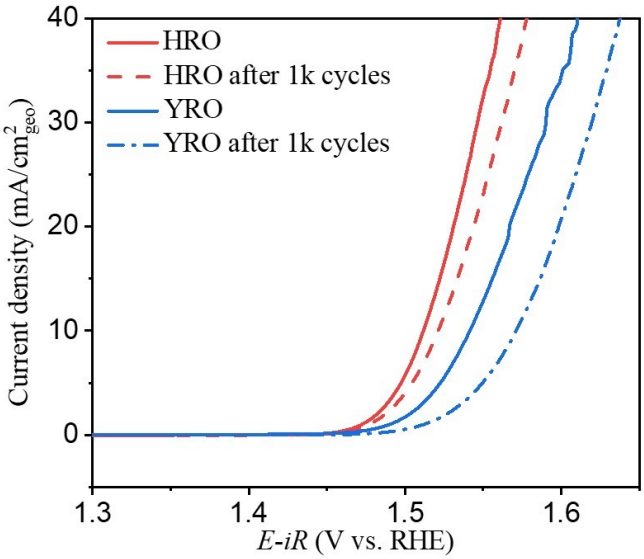

Fig. S9. LSV curves measured before and after 1000 CV cycles for HRO and YRO.

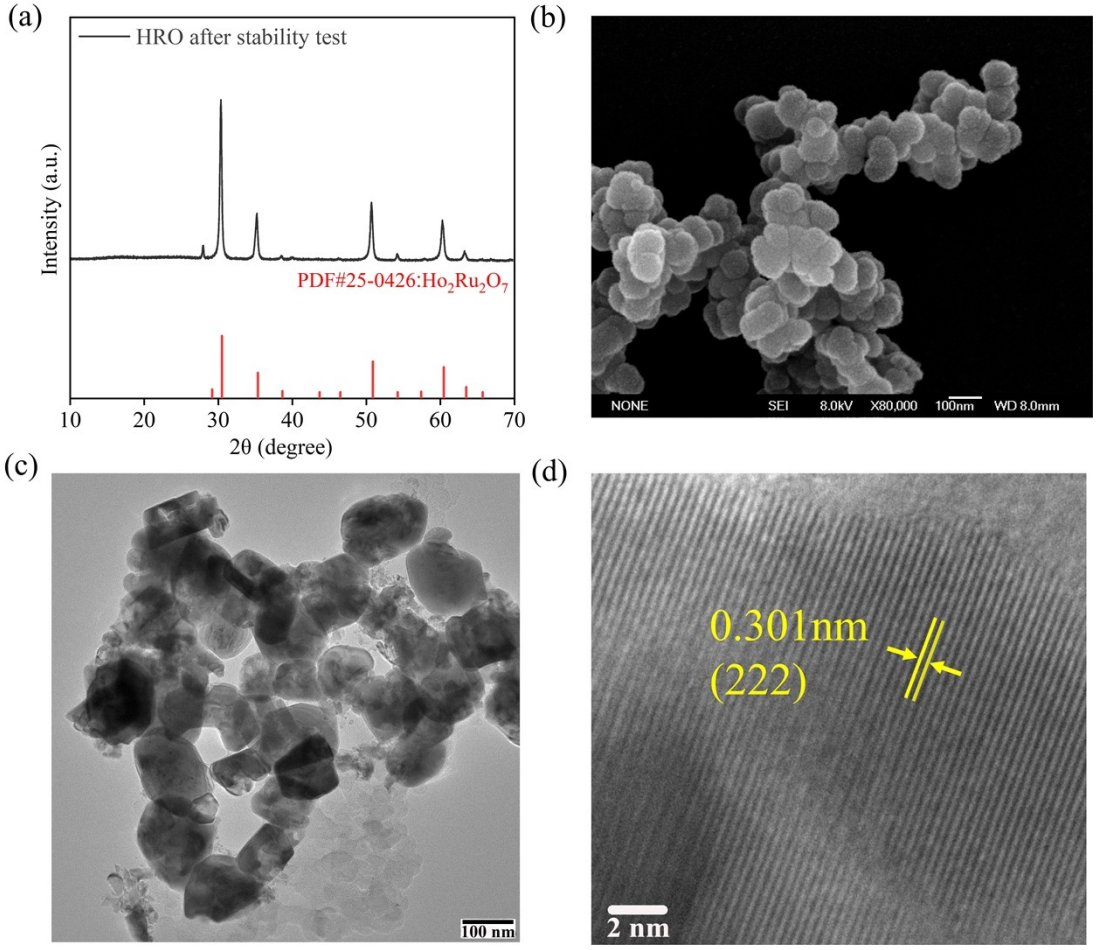

Fig. S10. Physical characterization for HRO after stability test. (a) XRD pattern; (b) SEM image; (c) TEM image; **(**d) HRTEM image.

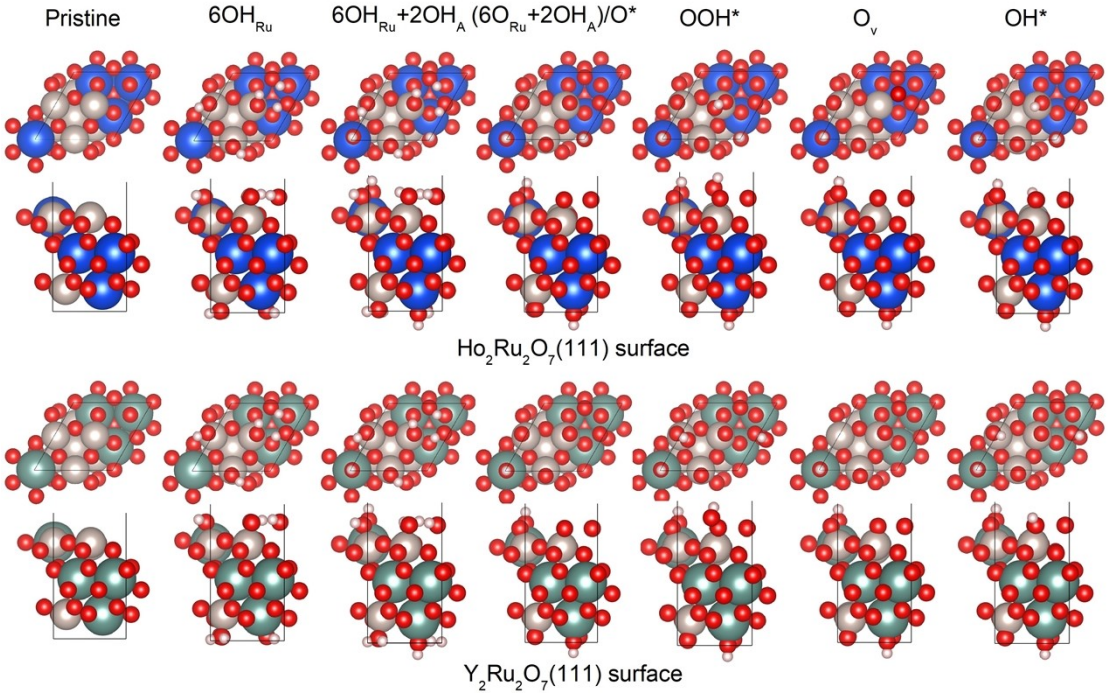

Fig. S11. The OER mechanism on the HRO (111) and YRO (111) surfaces.

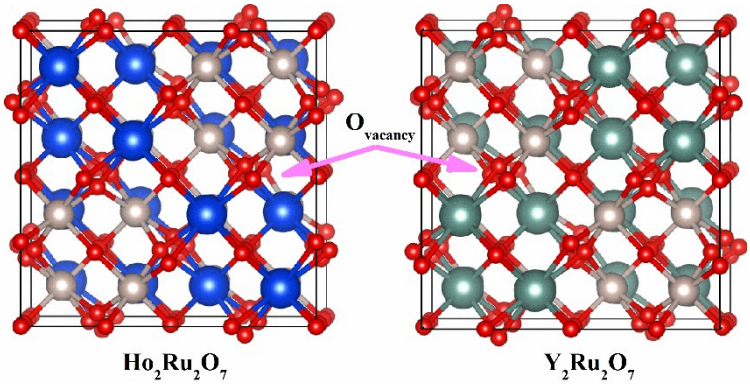

Fig. S12. The configurations of $Ho_2Ru_2O_7$ and $Y_2Ru_2O_7$, and the potential O vacancy positions in bulk structures for the formation energy of oxygen vacancy calculation.

Table S1. Detailed comparison information of electronegativity and radii for trivalent Ho and Y cations.[1,2]

	Electronegativity		Crystal Radius		Ionic Radius	
CN	HRO	YRO	HRO	YRO	HRO	YRO
6	1.433	1.340	1.041	1.040	0.901	0.900
7	1.403	1.314	--	1.100	--	0.960
8	1.377	1.291	1.155	1.159	1.015	1.019
9	1.353	1.272	1.216	1.215	1.072	1.175
10	1.334	--	1.260	--	1.120	--

Table S2. ICP analysis for HRO.

Element	Sample amount	Conversion content	Wt.%
Ho	9.5 mg	200526.3 mg/kg	20.05%
Ru	9.5 mg	111842.1 mg/kg	11.18%

Table S3. The ratio of all peaks in O 1s spectrum

		O_L	O_{sur}	O_V	O_{adv}	O_V/O_L
HRO	area	69076.1	32539.1	35486.6	22944.3	0.51
	ratio	43.2%	20.3%	22.2%	14.3%	
YRO	area	83072.5	36823.6	63298.4	21949.9	0.76
	ratio	40.5%	17.9%	30.9%	10.7%	

Table S4. ICP analysis of Ru^{3+} for HRO and YRO after stability test.

Sample	YRO	HRO
Concentration (mg/L)	1.05	0.91

Table S5. The O vacancy formation energy (Bader charge analysis)

	$E_{Ovcancay}$/eV	[a] d-band center/eV	[b] d-band center/eV	Band gap/eV	Magnetic moment/μ
YRO	1.58	-3.33	-4.37	0.648	1.682
HRO	4.18	-3.35	-4.42	0.645	1.684

*Bandgap and magnetic moments on Ru in bulk YRO and HRO.

[a] Bulk, [b] Surface of YRO and HRO

Table S6. Comparison of OER performance for pyrochlore oxides in acidic media.

Electrocatalyst	Supporter	Electrolyte	Overpotential (mV) @ 10 mA/cm^2	Tafel slope (mV/dec)	Stability	Reference
$Ho_2Ru_2O_7$	**GCE[1]**	**0.1 M $HClO_4$**	**280**	**36.86**	**60 h @ 1 mA cm^{-2}**	**This work**
	TFP[2]		**215**	**----**	**10 h @ 10 mA cm^{-2}**	
$Y_2Ru_2O_7$	**GCE**	**0.1 M $HClO_4$**	**312**	**42.91**	**2 h @ 10 mA cm^{-2}**	**This work**
$Y_{1.85}Zn_{0.15}Ru_2O_{7-\delta}$	AB[3]	0.5 M H_2SO_4	291	36.90	8 h @ 1 mA cm^{-2}	[3]
$Nd_2Ru_2O_7$	GCE	0.1 M $HClO_4$	310	58.48	8 h @ 1 A F^{-1}	[4]
$Sm_2Ru_2O_7$	GCE	0.1 M $HClO_4$	345	58.98	----	[4]
$Pr_2Ir_2O_7$	GCE	0.1 M $HClO_4$	295	----	3 h @ 10 mA cm^{-2}	[5]
$Y_{1.85}Ba_{0.15}Ru_2O_7$	GCE	0.5 M H_2SO_4	287	40.80	5 h @ 10 mA cm^{-2}	[6]
$Y_2[Ru_{1.6}Y_{0.4}]O_{7-\delta}$	GCE	0.1 M $HClO_4$	245	37.00	----	[7]
$Nd_2Ru_2O_7$	GCE	0.1 M $HClO_4$	342	41.00	1 h @ 10 mA cm^{-2}	[8]
$Gd_2Ru_2O_7$	GCE	0.1 M $HClO_4$	349	47.00	1 h @ 10 mA cm^{-2}	[8]
$Y_{1.7}Sr_{0.3}Ru_2O_7$	GCE	0.5 M H_2SO_4	264	44.8	28 h @ 10 mA cm^{-2}	[9]
$Y_2Ru_2O_{7-\delta}$	GCE	0.1 M $HClO_4$	300 mV @ 5 mA/cm^2	46	8 h @ 1 mA cm^{-2}	[10]

[1]GCE = glass carbon electrode, [2]TFP = Ti fiber paper, [3]AB = Acetylene black.

Reference

[1] K. Li, and D. Xue, *J. Phys. Chem. A*, 2006, **110**, 11332-11337.

[2] R. D. Shannon, *Acta Cryst.*, 1976, **A32**, 751.

[3] Q. Feng, Q. Wang, Z. Zhang, Y. Xiong, H. Li, Y. Yao, X.-Z. Yuan, M. C. Williams, M. Gu, H. Chen, H. Li, H. Wang, *Appl. Catal. B* 2019, **244**, 494.

[4] H. Liu, Z. Wang, M. Li, X. Zhao, X. Duan, S. Wang, G. Tan, Y. Kuang, X. Sun, *Sci. China Mater.* 2021, **64**, 1653.

[5] C. Shang, C. Cao, D. Yu, Y. Yan, Y. Lin, H. Li, T. Zheng, X. Yan, W. Yu, S. Zhou, J. Zeng, *Adv. Mater.* 2019, **31**, e1805104.

[6] Q. Feng, J. Zou, Y. Wang, Z. Zhao, M. C. Williams, H. Li, H. Wang, *ACS Appl. Mater. Interfaces* 2020, **12**, 4520.

[7] J. Kim, P. C. Shih, Y. Qin, Z. Al-Bardan, C. J. Sun, H. Yang, *Angew. Chem. Int. Ed. Engl.* 2018, **57**, 13877.

[8] M. A. Hubert, A. M. Patel, A. Gallo, Y. Liu, E. Valle, M. Ben-Naim, J. Sanchez, D. Sokaras, R. Sinclair, J. K. Nørskov, L. A. King, M. Bajdich, T. F. Jaramillo, *ACS Catal.* 2020, **10**, 12182.

[9] N. Zhang, C. Wang, J. Chen, C. Hu, J. Ma, X. Deng, B. Qiu, L. Cai, Y. Xiong, Y. Chai, *ACS Nano* 2021, **15**, 8537.

[10] J. Kim, P. C. Shih, K. C. Tsao, Y. T. Pan, X. Yin, C. J. Sun, H. Yang, *J. Am. Chem. Soc.* 2017, **139**, 12076.